



# Study on water and oxygen transfer characteristics of HT-PEM fuel cells

Hongbin He<sup>\*</sup>, Haisi Peng, Guangchao Li

Shenyang Aerospace University, China

## ARTICLE INFO

### Keywords:

Mass transfer  
HT-PEM fuel cells  
Cathode thickness  
Oxygen transmission

## ABSTRACT

In this study, a steady-state model is developed by combining mechanical, Navier–Stokes, Maxwell–Stefan, and Butler–Volmer equations. This model is then used to investigate the influences of diffusion layer thickness deformation under a specific assembly force on the porosity distribution as an indicator of fuel cell performance. The HT-PEM (high temperature proton exchange membrane) fuel cell model is built using COMSOL Multiphysics software, simulating the changes in diffusion layer porosity under different thicknesses of the diffusion layer, thus analyzing the trends in variation of water and oxygen concentration in the cathode diffusion layer. The battery has different current densities at different operating potentials. The influence of the working potential on the mass transfer concentration and the variation in the mass transfer concentration of the diffusion layer under the different areas of flow channel and flow ridge is discussed. The simulation results have a certain reference value for the optimization of mass transfer in a diffusion layer. The results reveal the combined effect of the assembly force and flow field, which makes the porosity distribution uneven and results in remarkable lateral current in the gas diffusion layer (GDL). The thicker the diffusion layer, the less oxygen consumed, and a large amount of oxygen is retained in the gaseous diffusion layer. It can be concluded that thicker diffusion layer is conducive to more uniform mass transfer and diffusion. These results can potentially be used to promote the performance and application of HT-PEMFC.

## 1. Introduction

In recent years, fuel cells have attracted extensive attention as a highly efficient and pollution-free device for energy conversion studied by many researchers. There are high expectations for HT-PEM fuel cells, due to their simple water management [1], strong tolerance [2], and great operating stability [3]. The gas diffusion layer inside the fuel cell is considered the most significant part of the fuel cell. As a skeleton, it supports the catalyst layer and also provides an effective channel for internal mass transfer and diffusion processes [4]. Therefore, we focus on enhancing the mass transfer efficiency of the gas diffusion layer, which is directly representative of fuel cell performance.

For years, many researchers have studied and achieved great progress in various aspects of the diffusion layer. Ozgur Delikaya et al. prepared a porous carbon nanofiber network as an electrode of polymer fuel cells, effectively improving the performance of the fuel cell [5]. Sun Hong et al. established a two-dimensional steady-state mathematical model to analyze the law of mass transfer and diffusion of water and oxygen in the cathode diffusion layer [6]. At the same time, through fluid dynamics analysis, simulation, and

<sup>\*</sup> Corresponding author.

E-mail address: [hehongbin@email.sau.edu.cn](mailto:hehongbin@email.sau.edu.cn) (H. He).

other methods, some researchers have investigated diffusion layer thickness, porosity, and other factors affecting the performance of fuel cells [7]. O Shamardina et al. built a two-dimensional steady-state model to analyze the influence of high-temperature fuel cells' performance by exploring the cathode mass transfer and voltage loss [8]. Zhang et al. established out a two-dimensional two-phase flow model to discuss the water transfer and distribution characteristics in two-dimensional space [9]. S Park et al. reviewed various types of diffusion layers from the perspective of materials and then discussed the future development prospects of diffusion layers [10]. The pore structure with a commercial gas diffusion layer through X-ray scanning was mentioned by IV Zenyuk et al. and their report serves as a reference for the considered design of fuel cell diffusion layer [11]. Y Wang et al. simulated the startup process of the fuel cell, analyzed the influence of gas flow direction on battery startup and proposed the best method for the startup of high-temperature fuel cells [12]. Xia et al. created a three-dimensional fuel cell model to optimize the porosity and thickness of the diffusion layer of the cell and achieved a 7.7% enhancement in performance. At the same time, they systematically analyzed the influence of various parameters on the performance of high-temperature fuel cells [13,14]. Wang et al. calculated the optimal thickness of a high-temperature fuel cell catalyst layer using a genetic algorithm method, which improved the fuel cell performance by 6.8% [15]. Li et al. used the variational principle to optimize the porosity distribution of the diffusion layer of high-temperature fuel cells. The necessity for optimizing the parameters of the electrode diffusion layer was pointed out [16]. Xu et al. aimed at the aspirated fuel cells as their research direction to analyze the flow field parameters of batteries from both experimental and simulation tests, thereby obtaining the optimal opening rate of batteries [17]. Zhu et al. constructed a digital drive model for high-temperature fuel cells and conducted detailed analysis of the influence of fuel cell parameters [18]. Chun et al. used X- $\mu$  CT and other methods to analyze the pore characteristics of high-temperature polymer electron fuel cells and studied the influence of cathode pore characteristics on the battery performance [19]. In terms of the stress deformation of diffusion layer, Atifi et al. conducted numerical analysis of the influence of contact pressure on the deformation of the diffusion layer [20].

In this study, a high-temperature fuel cell model with a three-dimensional single-channel under a steady state is constructed. The effects of different diffusion layer thickness parameters on material transport and fuel cell performance under the condition of 2 MPa stress are analyzed. The main research contents include the analysis of the water and oxygen contents in the fuel cell cathode. Then, the volt-ampere performance curve of the fuel cell is comprehensively evaluated. This study has a certain significance as a reference for the optimization of performance parameters of high-temperature fuel cells under the condition of preload.

## 2. Model and calculation method

### 2.1. Geometrical model

According to the structure and electrochemical characteristics of HT-PEM fuel cells, a three-dimensional single-channel HT-PEM fuel cell model under a steady state is established. The geometric structure of the model is shown in Fig. 1. The fuel cell is composed of seven parts: the cathode flow channel, cathode diffusion layer, cathode catalyst layer, proton exchange membrane, anode catalyst layer, anode diffusion layer, and anode flow channel.

The inlet and outlet are only the positions at the boundary of gas inflow and outflow in the model, which is different from the actual situation of oxygen inflow and outflow in the experiment. To visually analyze the changes in oxygen concentration in this model, we set the initial oxygen inflow to a fixed value.

### 2.2. Mathematical model

This model uses the porous media, secondary current distribution, and solid mechanics modules to analyze the mass transfer process, electrochemical reaction, diffusion layer deformation, and porosity change. The details are presented in the following.

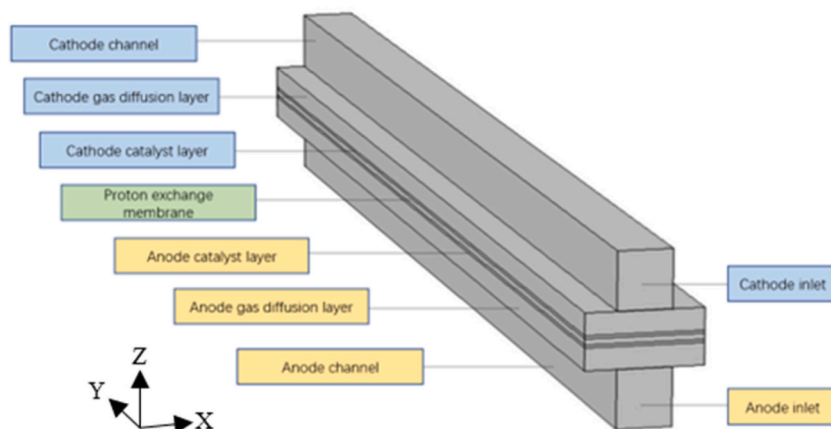


Fig. 1. HT-PEM fuel cell geometric model structure diagram.

### 2.2.1. The porous media mode

The porous media module is mainly used to describe the distribution of mass transfer in the diffusion and catalyst layers, thus acting on the flow channel, gas diffusion layer, and catalyst layer region. The momentum transfer is calculated using the Navier–Stokes equation, and the mass conservation of the model is ensured by the continuous equation. The gas mass transfer in the model is assumed to be layered and incompressible. The Maxwell–Stefan equation is provided to describe the multi-component diffusion in the diffusion layer. The specific calculation equations are as follows.

The equation of Navier–Stokes is expressed as equations (1) and (2):

$$\rho(u \cdot \nabla)u + \nabla p - \nabla \cdot \eta(\nabla u + (\nabla u)^T) = 0 \tag{1}$$

$$\nabla \cdot (\rho u) = 0 \tag{2}$$

The equation of Maxwell–Stefan is shown as equation (3):

$$\nabla \cdot \left( -\rho \omega_i \sum_j \left( D_{ij} \nabla x_j + (x_j - \omega_j) \frac{\nabla p}{p} \right) + \rho \omega_i u \right) = 0 \tag{3}$$

in this equation,  $\rho$  is the density,  $u$  is the velocity,  $\omega$  is the mass fraction,  $D$  is the diffusion coefficient, and  $p$  is the pressure.

### 2.2.2. Electrochemical model

The secondary current distribution module is used to discuss the electrochemical parameters of the model. Ohm’s law and charge conservation are coupled by the secondary current distribution. The aim is to define the transfer of charged ions in a one-component electrolyte and the conduction of current across the electrode while taking into account the effect of hyperactivation potential. The Butler–Volmer and Tafel expressions are executed to determine the secondary current distribution. The Butler–Volmer equation is performed to describe the concentration dependence on the exchange current density, as seen in equation (4).

$$j = j_0 \left( \frac{c_R^*}{c_R^{0*}} e^{anF\eta/(RT)} - \frac{c_P^*}{c_P^{0*}} e^{-(1-\alpha)nF\eta/(RT)} \right) \tag{4}$$

For the equation of Tafel,  $\eta_{act}$  is considered relatively large in the model and, therefore, the second exponential term in the Butler–Volmer equation can be ignored. Here can be simplified as shown in equations (5) and (6):

$$j = j_0 e^{anF\eta_{act}/(RT)} \tag{5}$$

$$\eta_{act} = -\frac{RT}{anF} \ln j_0 + \frac{RT}{anF} \ln j \tag{6}$$

$j_0$  and  $\alpha$  can be obtained by fitting  $\eta_{act}$  to  $\ln j$ , and the equation can be written in the following form of equation (7):

$$\eta_{act} = a + b \ln j \tag{7}$$

where  $b$  is named the Tafel slope.

The charge conservation can be defined as equations (8) and (9):

$$\nabla \cdot (\sigma_s \nabla \phi_s) + S_{\phi_s} = 0 \tag{8}$$

$$\nabla \cdot (\sigma_m \nabla \phi_m) + S_{\phi_m} = 0 \tag{9}$$

in the formula,  $\eta$  represents the lost voltage,  $n$  represents the number of electrons transferred in the reaction,  $c^* R$  and  $c^* P$  represent the actual surface concentration of the substance with finite rate in the reaction, and  $j_0$  is the actual measured value at the reference point, namely the exchange current density at a standard concentration. The concentration of reactants and products here are denoted by  $c^{0*}R$  and  $c^{0*}P$ , respectively, where  $\sigma$  stands for the electrical conductivity.

### 2.2.3. Mechanical model

A solid mechanical field is applied to the cathode diffusion layer and anode diffusion layer of the fuel cell to describe the compression state of the gas diffusion layer under assembly force. This study describes the three-dimensional stress distribution of the diffusion layer from the aspects of statics, geometry, and physics such that it can be divided into the three equations (10)–(12) as follows [21]:

$$\text{Equilibrium differential equation: } \frac{\partial \sigma_{ii}}{\partial x_i} + \frac{\partial \tau_{ij}}{\partial x_j} + \frac{\partial \tau_{ik}}{\partial x_k} + F_i = 0 \tag{10}$$

$$\text{Geometric equation: } \frac{\partial^2 \varepsilon_{ii}}{\partial x_j^2} + \frac{\partial^2 \varepsilon_{ij}}{\partial x_i^2} - \frac{\partial^2 \gamma_{ij}}{\partial x_k^2} = 0 \tag{11}$$

$$\text{Physical equation: } \sigma_{ii} = \lambda e + 2G\varepsilon_{ii} \tag{12}$$

$\sigma_{ii}$  is normal stress,  $\tau_{ij}$  is shear stress,  $F_i$  is volume force,  $\varepsilon_{ii}$  is positive strain,  $G$  is shear elastic modulus,  $\lambda$  is the Lamet constant, where are presented in equations (13)–(15):

$$G = \frac{E}{2(1 + \mu)} \quad (13)$$

$$\lambda = \frac{\mu E}{(1 + \mu)(1 - 2\mu)} \quad (14)$$

$$\gamma_{ij} = \tau_{ij}/G, e = \varepsilon_i + \varepsilon_j + \varepsilon_k \quad (15)$$

where  $E$  represents Young's modulus,  $\mu$  is Poisson's ratio, and  $i, j$ , and  $k$  represent the x, y, and z directions, respectively.

#### 2.2.4. Calculation method

In this study, the COMSOL Multiphysics software is used for simulation calculation. Before calculation, the following assumptions are upheld during the calculation process: (1) all operations are performed under the conditions of a constant temperature and a steady state; (2) the fluid in the passage is laminar flow; and (3) porous media are defined as isotropic; (4) the gas mixture used in the operation of the battery model is considered as an ideal gas, which is not affected by gas compression.

By the simulation calculation, parameters need to be firstly input (as shown in Table 1). Then, the grid is divided, where 1/8 of the length of the flow channel is selected as the maximum element size at the upper and lower boundaries of the diffusion layer. The number of elements at the left and right boundaries of the flow channel is 8. The number of elements at the left and right boundaries of the gas diffusion layer is also 8. The number of elements at the left and right boundaries of the electrode is 6. The number of elements at the left and right boundaries of the proton exchange membrane is 3, and the remaining boundaries are mapped and swept. The number of fixed elements is 8, and the ratio of elements to elongate is 2. The above method not only guarantees the accuracy of the calculation results but also efficiently minimizes the operation time.

Finally, the boundary conditions will be entirely set up. According to the test gas flow rate per minute combined with the model geometry, the model inflow boundary velocity of the cathode and the anode are set as 0.5 and 0.2 m/s, respectively. A fixed constraint is set at the lower boundary of the gas diffusion layer and a boundary load is applied to the upper boundary.

### 3. Results and discussion

#### 3.1. Model validity and fuel cell volt-ampere characteristics analysis

Aiming to validate the model, a self-designed flow field plate is used in this HT-PEM fuel cell, and the size of the flow field plate corresponds to that used in the model. Using platinum-carrying carbon paper as the electrode, platinum-supported carbon paper was coated with catalyst by spraying process. In this test, carbon paper loaded with platinum catalyst was purchased for testing. The electrode reaction area is 4 cm<sup>2</sup>, and the platinum loading is 0.5 mg/cm<sup>2</sup>. The ab-polybenzimidazoles(ab-PBI) membrane was used as the proton exchange membrane. First of all, the membrane was acidified by soaking in 85% concentrated phosphoric acid for 18 h at 140 °C, and the excess phosphoric acid on the membrane surface can then be removed with dust-free paper. Through this method, the membrane conductivity can be effectively improved, and the role of proton transfer can be provided to the membrane. During

**Table 1**  
Calculation parameters.

Parameters/Unit	Value
length of channel/m	$2 \times 10^{-2}$
width of channel/m	$8 \times 10^{-4}$
height of channel/m	$10^{-3}$
width of flow ridge/m	$9 \times 10^{-4}$
thickness of gas diffusion layer/m	$3 \times 10^{-4}$ , $3.5 \times 10^{-4}$ , $4 \times 10^{-4}$ , $4.5 \times 10^{-4}$ , $5 \times 10^{-4}$
thickness of porous electrode (m)	$15 \times 10^{-6}$
thickness of membrane (m)	$1 \times 10^{-4}$
porosity of diffusion layer	0.4
conductivity of diffusion layer ( s/m )	222 [22]
membrane conductivity (s/m)	9.825 [23]
mass fraction of hydrogen inlet	0.743
mass fraction of water inlet	0.023
mass fraction of oxygen inlet	0.228
Fuel cell temperature (K)	453
Relative pressure (Pa)	$1.013 \times 10^5$
Cell voltage (V)	0.4
Young's modulus of diffusion layer (Pa)	$5.54 \times 10^6$
Poisson's ratio of diffusion layer	0.24 [23]
pressure of flow ridge (Pa)	$2 \times 10^6$

assembly, a pretension wrench is used to set the pretension to ensure that the assembly force of the fuel cell is suitable. XBL50-150-800 fuel cell test system is used for the test. The test system consists of an air supply system, a humidification preheating system, a battery test system, and a fuel cell monomer. The schematic diagram of the test system is shown in Fig. 2. During the test, the battery needs to be preheated first. When the temperature reaches 120 °C, the electronic load is applied to the fuel cell, and the polarization curve test is started until the battery temperature rises up to 180 °C.

A numerical polarization curve of the HT-PEMFC with the same structure and operating parameters as used in above experiments is obtained by the model.

As shown in Fig. 3, the variation in voltammetry characteristic curves under different diffusion thicknesses is presented. The voltammetry characteristic curves with a thickness of 0.35 mm are measured experimentally. The simulation results are close to the experimental trend, thus indicating the validity of the simulation results. It can be seen from the figure that the influence of diffusion layer thickness on fuel cell performance is not evident under high potential conditions. In contrast, under low voltage conditions, with the increase of diffusion layer thickness, the current density gradually decreases.

### 3.2. Influence of diffusion layer thickness on porosity distribution

It is found that when the assembly prestress is 2 MPa, the average current density reaches the maximum value. This means that 2 MPa is the optimum assembly prestress for achieving the highest performance of the PEM fuel cell, as in the previous study. Therefore, in this study, the thickness of the diffusion layer is directly changed. When the pressure is 2 MPa, the variation rule for the diffusion layer porosity is analyzed and discussed. It can be seen from Fig. 4 that for the same applied load, the diffusion layer porosity shows a variation trend of basically remaining the same. However, due to the different thicknesses of the diffusion layer, the results clearly show that when the thickness of the diffusion layer increases, the distance and side length required for mass transfer and the changed area of porosity also are increased due to extrusion. This means that the area of mass transfer inhibited is also increased, resulting in difficulties for the diffusion of mass transfer. This is the basis for the subsequent research in this paper, where we attempt to analyze fuel cell performance by studying the influence of diffusion layer thickness on the transmission of oxygen and water separately.

### 3.3. Influence of diffusion layer thickness on oxygen transmission

Fig. 5 shows the variation in oxygen concentration at the model inflow boundary and model outflow boundary of the diffusion layer, and the thickness of the diffusion layer ranges from 0.3 to 0.5 mm. It can be observed that the oxygen concentration at the model outflow boundary tends to be enhanced with an increase in the thickness of the diffusion layer. This indicates that a thinner diffusion layer can lead to the high efficiency of oxygen diffusion and reaction. The comparison of oxygen consumption at model inflow boundary and model outflow boundary shows that the thinner diffusion layer consumes a large amount of oxygen in the reaction. The thinner the diffusion layer, the higher the molar concentration of oxygen at the entrance and exit with the increase in test potential, which is considerably strengthened at the exit. This is because when the potential increases, the electrochemical reaction rate decreases, and thus, the amount of consumed oxygen decreases.

According to Fig. 6, when the thickness of the diffusion layer is 0.35 mm, there is clear variation in oxygen molarity along the X direction under different test potentials at the model outflow boundary of the model, which is analyzed and discussed. As can be seen, there is higher oxygen concentration in the diffusion layer below the flow passage than below the flow ridge. This can be explained by

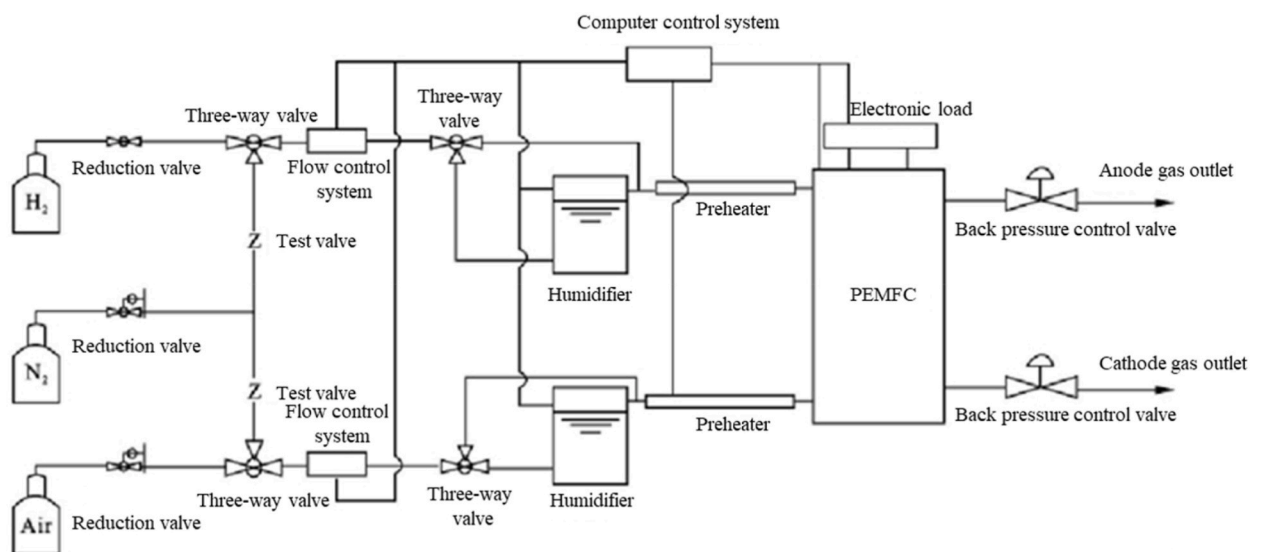


Fig. 2. Schematic diagram of electrochemical test system.

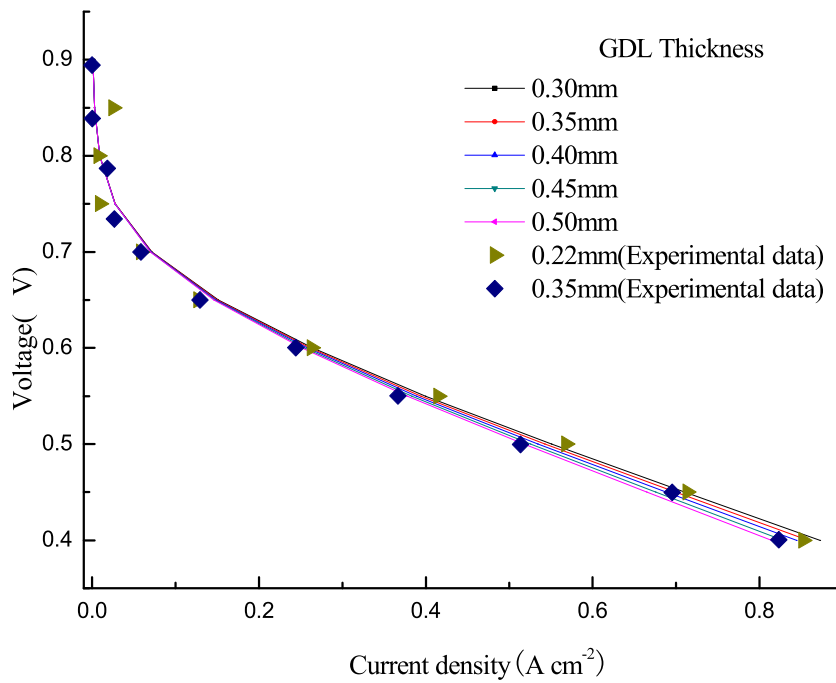


Fig. 3. Voltammetry curves under different layer thicknesses.

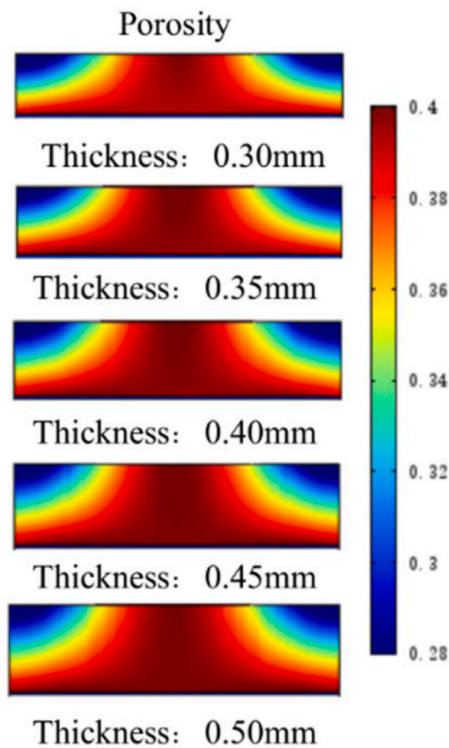


Fig. 4. Porosity distribution under different diffusion layer thicknesses.

the oxygen in the area below the flow passage being more likely to spread into the diffusion layer, while it is relatively more difficult to enter the area below the flow ridge. With the increase in the test potential, the difference between the molar concentration of oxygen at the model outflow boundary and the ridge area gradually decreases. This means that less oxygen is consumed during the reaction, and

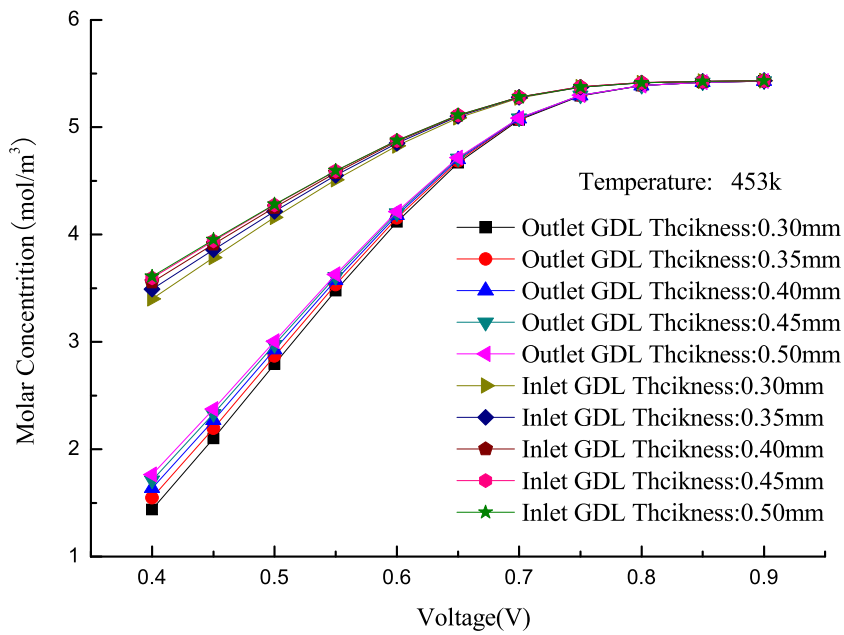


Fig. 5. Variations in oxygen molar concentration with electric potential under different diffusion thicknesses.

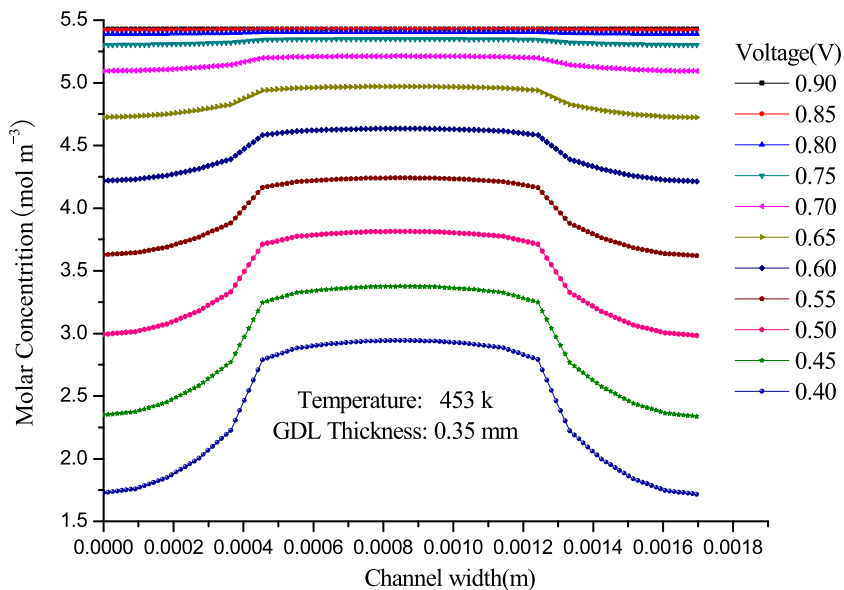
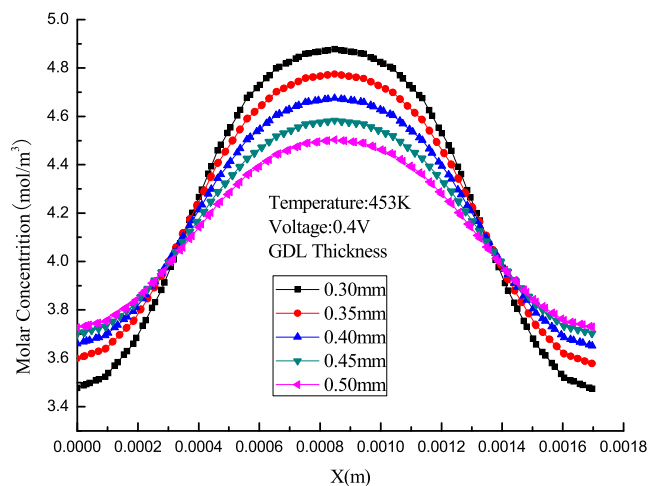


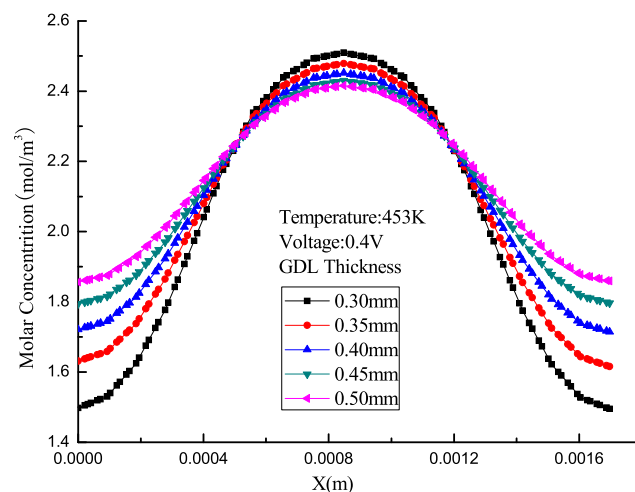
Fig. 6. Variations in molar concentration of oxygen at the model outflow boundary under different electric potentials.

a large amount of oxygen flows into the diffusion layer below the ridge. When the potential is above 0.8 V, there is no difference in oxygen concentration between the area below the flow passage and the flow ridge.

As can be seen from Fig. 7 (a) and (b), at the central section of the diffusion layer, the differences in molar concentration of oxygen at the model inflow boundary and model outflow boundary of the diffusion layer are carried out. It is obvious from Fig. 7(a) that in the area below the flow passage, the molar concentration of oxygen presents a downward trend as the thickness of the diffusion layer increases. The increase in diffusion layer thickness does not favor oxygen transfer. In the part below the flow ridge on both sides of the diffusion layer, especially on both sides of the diffusion layer, the molar concentration of oxygen is considerably enhanced with the increasing thickness of the diffusion layer. This can be explained by the thinner diffusion layer resulting in larger changes in the porosity under the same preloading pressure. It can be seen clearly that the thinner diffusion layer presents an obvious decreasing trend in the oxygen concentration, indicating that the decrease in the porosity results in increased resistance toward oxygen transfer.



(a) Molar concentration of oxygen at the model inflow boundary.



(b) Molar concentration of oxygen at the model outflow boundary.

**Fig. 7.** Molar concentration of oxygen at the center of diffusion layer under different thicknesses of diffusion layer, (a) at the model inflow boundary, (b) at the model outflow boundary.

### 3.4. Influence of diffusion layer thickness on water molarity distribution

At the central section of the diffusion layer, the comparison of the results for the water molarity is shown in Fig. 8. With the increase in electric potential, the observations of water molar concentration at the model inflow boundary and model outflow boundary are described carefully. At both the inflow and outflow boundaries, the results of the molar concentration of water present an apparent decreasing trend. It is obvious from Fig. 8 that compared with the molar concentration at the model inflow boundary, this decreasing tendency becomes much stronger at the model outflow boundary. A reasonable explanation is that as the potential increases, the reaction rate decreases, and then less water vapor is produced. Under the different diffusion layer thicknesses, a thicker for the inflow diffusion layer results in the lower molar concentration of water. This can be explained as follows: The thicker diffusion layer is not conducive to water transfer. In contrast, the thinner diffusion layer leads to higher molar concentration of water. These results mean that in the thinner diffusion layer model, the reaction is performed sufficiently and robustly, which is more suitable for producing much more water.

Fig. 9 shows the distribution of water concentration at the gas outlet of cathode under different potentials when the diffusion layer thickness is 0.35 mm. It can be concluded that the molar concentration of the water is lower below the flow passage than below the flow ridge. With the increase in electric potential, the molar concentration of water at the model outflow boundary of the diffusion layer is decreased. The concentration difference in the diffusion layer area between the downward arc of the flow passage and the downward arc of the flow ridge is becoming shorter. This further indicates that when the fuel cell operating potential increases, the reaction rate decreases, thus resulting in a decrease in the gas concentration.

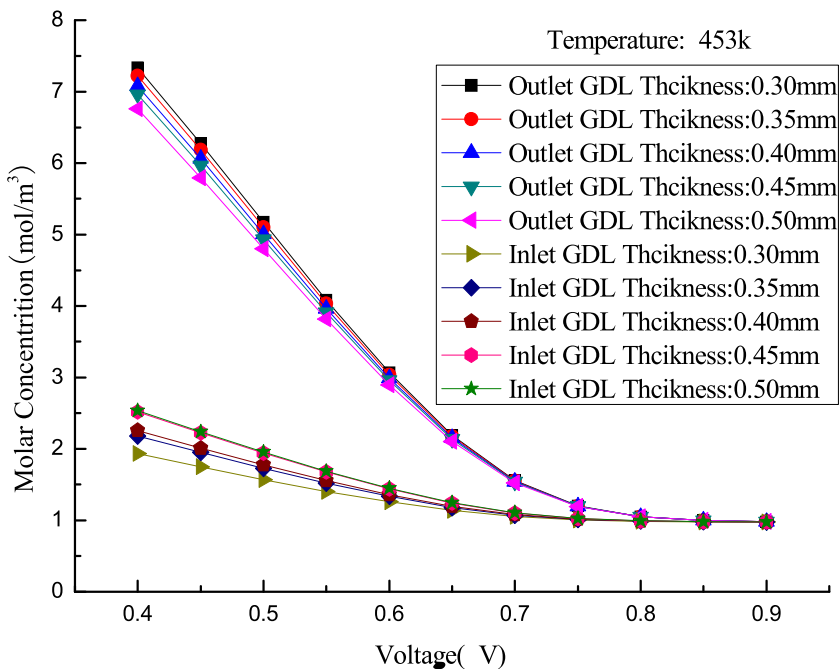


Fig. 8. Distribution of molarity of water with electric potential.

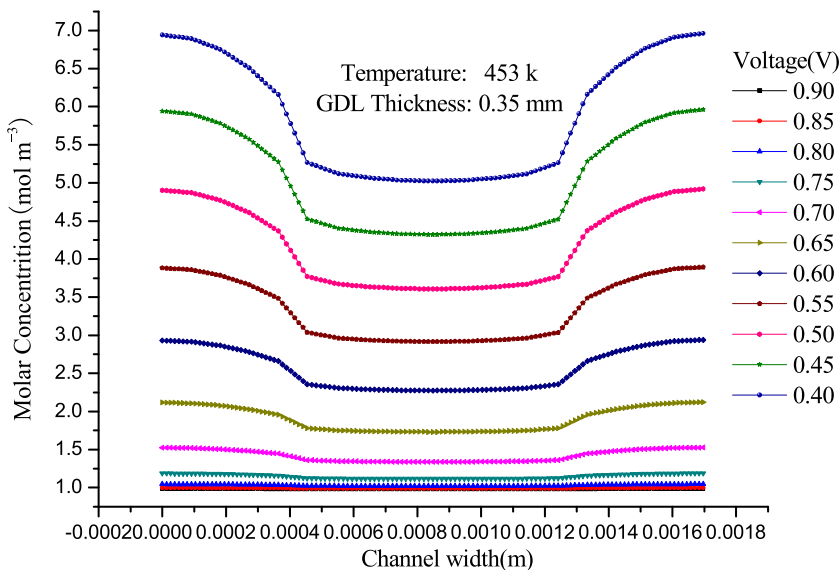
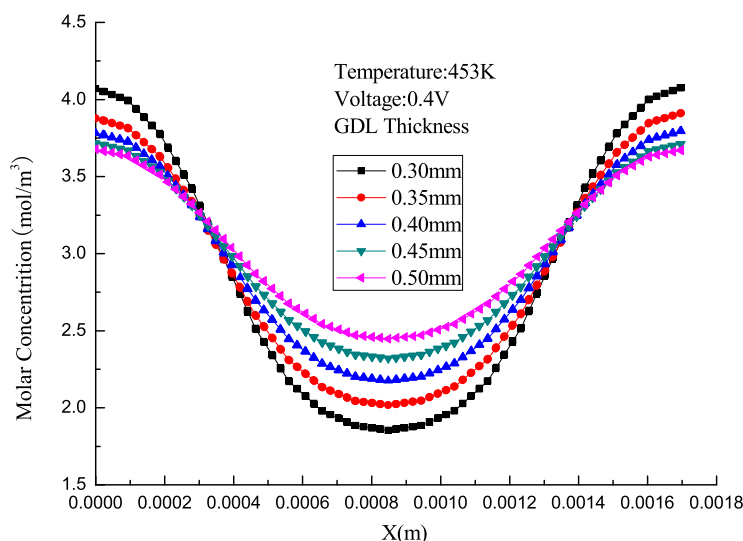
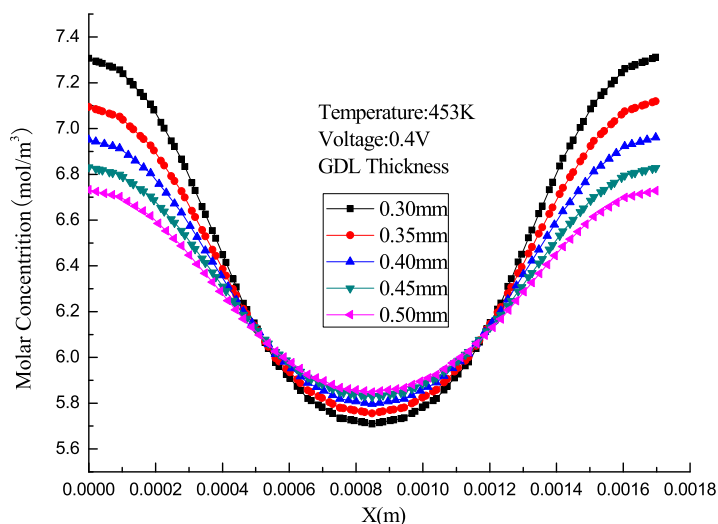


Fig. 9. Changes in molar concentration of water at the model outflow boundary under different electric potentials.

Fig. 10 (a) and (b) present the distributions of molarity of water at the model inflow boundary and model outflow boundary under different diffusion thicknesses. It can be clearly seen that with the increase in the diffusion layer thickness, the molarity of water in the area below the flow passage shows an increasing trend. In contrast, it shows a decreasing trend below the flow ridge. These results clearly indicate that as the reaction progresses, the generated water is more likely to diffuse toward the ridge area, as the space below the flow passage is occupied by oxygen. The larger thickness of the diffusion layer leads to a smaller concentration difference between the flow passage and the flow ridge. This indicates that the enlargement of the thickness of the diffusion layer is conducive to uniformity in the performance in terms of mass transfer and diffusion. To conclude, it is evident that the implementation of an assembly force has a noteworthy influence on the trend of substance concentration. However, under the current assembly force condition, material transport remains the primary factor contributing to changes in material concentration gradient. As discussed in this study, the thickness of the gas diffusion layer remains the dominant factor affecting material concentration trend when the assembly force



(a) Molarity distribution of water at the model inflow boundary.



(b) Molarity distribution of water at the model outflow boundary.

**Fig. 10.** Distribution of water molarity with different layer thicknesses, (a) at the model inflow boundary, (b) at the model outflow boundary.

remains constant.

Fig. 11 shows the change in water formation concentration and oxygen consumption concentration in the center line of the cathode gas diffusion layer. It can be seen from the figure that the ratio of oxygen consumption concentration to water production concentration is slightly less than two at the selected cross-section position. However, with the increase in cathode thickness, oxygen consumption, and water production decreased first and then increased. For the above phenomenon, it can be seen that due to the influence of material transport, the transport efficiency of water below the flow channel is better. Hence, the concentration of water generation is slightly less than two times oxygen consumption. However, due to the influence of the thickness of the diffusion layer, the larger the thickness, the greater the concentration gradient. When the thickness of the diffusion layer is increased to 0.5 mm, the diffusion efficiency of water molecules decreases more, resulting in more water deposited at the selected position, which leads to this trend of concentration change.

#### 4. Conclusion

In this study, a three-dimensional steady-state HT-PEM fuel cell model is constructed using COMSOL Multiphysics software. The changes in diffusion layer porosity under different diffusion layer thicknesses are simulated, and the variation trends in water and oxygen concentrations in the cathode diffusion layer are also studied. Through numerical calculation and analysis under different assembly

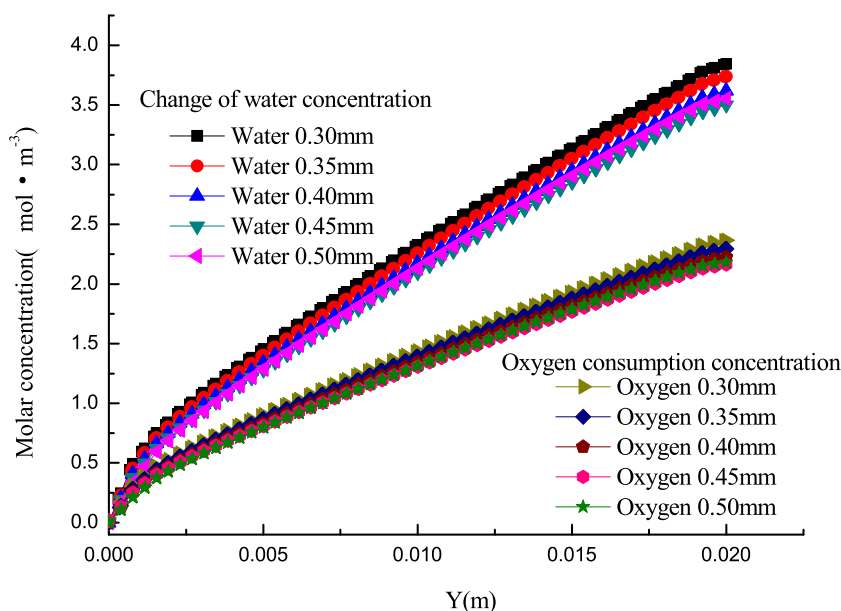


Fig. 11. Concentration of water generation and oxygen consumption in the center line of the cathode gas diffusion layer.

force conditions, we have clarified the influence of different gas diffusion layer thickness on the performance of HT-PEMFC. Therefore, the significance of this study is to guide the selection of carbon paper materials for cathode diffusion layer. The conclusions are as follows.

- (1) Under the same assembly force, the thinner diffusion layer has a larger proportion of deformation areas, and the obstruction of material transport in local areas is more obvious.
- (2) As the working potential increases, the molar concentration of oxygen increases, and the molar concentration of water decreases, with reduced oxygen consumption. This indicates that the lower of potential results in the higher current density, which leads to the faster rates of reaction and oxygen consumption. The thicker diffusion layer causes less oxygen to be consumed, which means much more oxygen is retained in the gaseous diffusion layer.
- (3) As the thickness of the diffusion layer is increased, the mass transfer concentration difference in the diffusion layer area below the flow passage and the flow ridge shows apparent decreases. This can be explained by the thicker diffusion layer being conducive to more uniform mass transfer and diffusion. The thicker diffusion layer can contribute to the accumulation of water in the electrode, which is less likely to cause the blockage of material transmission due to the high local concentration. However, it is also concluded that the extension of the transmission path may worsen the overall performance of the fuel cell.

#### Author contribution statement

Hongbin He, Haisi Peng: Conceived and designed the experiments; Performed the experiments; Wrote the paper.  
Guangchao Li: Analyzed and interpreted the data.

#### Data availability statement

Data will be made available on request.

#### Additional information

No additional information is available for this paper.

#### Funding

This research was funded by the Department of Education of Liaoning province, grant number JYT2020054.

#### Declaration of competing interest

The authors declare that they have no known competing financial interests or personal relationships that could have appeared to

influence the work reported in this paper.

## References

- [1] R. Abdul, L. Quan, C. Zhang, H. Siew, A review on modelling of high temperature proton exchange membrane fuel cells, *Int. J. Hydrogen Energy* 42 (5) (2017) 3142–3165.
- [2] C. De Beer, P.S. Barendse, P. Pillay, et al., Online diagnostics of HTPEM fuel cells using small amplitude transient analysis for CO poisoning, *IEEE Trans. Ind. Electron.* 62 (8) (2015) 5175–5186.
- [3] R.E. Rosli, A.B. Sulong, W.R.W. Daud, et al., A review of high-temperature proton exchange membrane fuel cell (HT-PEMFC) system, *Int. J. Hydrogen Energy* 42 (14) (2017) 9293–9314.
- [4] D. Úbeda, F.J. Pinar, P. Cañizares, et al., An easy parameter estimation procedure for modeling a HT-PEMFC, *Int. J. Hydrogen Energy* 37 (15) (2012), 11308.
- [5] Ö. Delikaya, N. Bevilacqua, L. Eifert, et al., Porous electrospun carbon nanofibers network as an integrated electrode@ gas diffusion layer for high temperature polymer electrolyte membrane fuel cells, *Electrochim. Acta* 345 (2020), 136192.
- [6] H. Sun, C. Xie, H. Chen, A. Saif, A numerical study on the effects of temperature and mass transfer in high temperature PEM fuel cells with ab-PBI membrane, *Appl. Energy* 160 (2015) 937–944.
- [7] E. Carcadea, M. Varlam, D. Ingham, et al., The effects of cathode flow channel size and operating conditions on PEM fuel performance: a CFD modelling study and experimental demonstration, *Int. J. Energy Res.* 42 (8) (2018) 2789–2804.
- [8] O. Shamardina, A. Chertovich, A.A. Kulikovskiy, et al., A simple model of a high temperature PEM fuel cell, *Int. J. Hydrogen Energy* 35 (18) (2010) 9954–9962.
- [9] C. Zhang, L. Zhang, W. Zhou, Y. Wang, S. Chan, Investigation of water transport and its effect on performance of high-temperature PEM fuel cells, *Electrochim. Acta* 149 (2014) 271–277.
- [10] S. Park, J.W. Lee, B.N. Popov, A review of gas diffusion layer in PEM fuel cells: materials and designs, *Int. J. Hydrogen Energy* 37 (7) (2012) 5850–5865.
- [11] I.V. Zhenyuk, D.Y. Parkinson, L.G. Connolly, et al., Gas-diffusion-layer structural properties under compression via X-ray tomography, *J. Power Sour.* 328 (2016) 364–376.
- [12] Y. Wang, D.U. Sauer, S. Koehne, et al., Dynamic modeling of high temperature PEM fuel cell start-up process, *Int. J. Hydrogen Energy* 39 (33) (2014) 19067–19078.
- [13] L. Xia, M. Ni, Q. He, et al., Optimization of gas diffusion layer in high temperature PEMFC with the focuses on thickness and porosity, *Appl. Energy* 300 (2021), 117357.
- [14] T. Huang, J. Huang, M. Feng, et al., Optimization of the thickness of catalytic layer for Ht-pemfcs based on genetic algorithm, *Energy Rep.* 8 (2022) 12905–12915.
- [15] Y. Wang, L. Yue, S. Wang, New design of a cathode flow-field with a sub-channel to improve the polymer electrolyte membrane fuel cell performance, *J. Power Sour.* 344 (2017) 32–38.
- [16] Y. Li, F. Yuan, R. Weng, et al., Variational-principle-optimized porosity distribution in gas diffusion layer of high-temperature PEM fuel cells, *Energy* 235 (2021), 121350.
- [17] X. Xu, W. Yang, X. Zhuang, et al., Experimental and numerical investigation on effects of cathode flow field configurations in an air-breathing high-temperature PEMFC, *Int. J. Hydrogen Energy* 44 (45) (2019) 25010–25020.
- [18] G. Zhu, W. Chen, S. Lu, et al., Parameter study of high-temperature proton exchange membrane fuel cell using data-driven models, *Int. J. Hydrogen Energy* 44 (54) (2019) 28958–28967.
- [19] H. Chun, D.H. Kim, H.S. Jung, et al., Effects of gas-diffusion layer properties on the performance of the cathode for high-temperature polymer electrolyte membrane fuel cell, *Int. J. Hydrogen Energy* 71 (19) (2023) 27790–27804.
- [20] A. Atifi, K. El Bikri, M. Ettouhami, Numerical simulation of effect of contact pressure on gas diffusion layers deformation of a PEM fuel cell, in: *MATEC Web of Conferences* vol. 286, EDP Sciences, 2019, p. 09006.
- [21] K. Oh, P. Chippar, H. Ju, Numerical study of thermal stresses in high-temperature proton exchange membrane fuel cell (HTPEMFC), *Int. J. Hydrogen Energy* 39 (2014) 2785–2794.
- [22] H.L. Lin, T.L. Yu, W.K. Chang, et al., Preparation of a low proton resistance PBI/PTFE composite membrane, *J. Power Sour.* 164 (2) (2007) 481–487.
- [23] Y. Zhou, K. Jiao, Q. Du, et al., Gas diffusion layer deformation and its effect on the transport characteristics and performance of proton exchange membrane fuel cell, *Int. J. Hydrogen Energy* 38 (29) (2013) 12891–12903.